ELSEVIER

Restricted diffusion in a model acinar labyrinth by NMR: Theoretical and numerical results

D.S. Grebenkov [a,b,*], G. Guillot [b], B. Sapoval [c,d]

[a] *Dipartimento di Scienze Fisiche, Università di Napoli Federico II Complesso universitario Monte S. Angelo, Via Cintia, 80126 Naples, Italy*
[b] *Unité de Recherche en Résonance Magnétique Médicale, UMR8081 CNRS—Université Paris-Sud, Bât 220, 91405 Orsay, France*
[c] *Laboratoire de Physique de la Matière Condensée, UMR7643 CNRS—Ecole Polytechnique, 91128 Palaiseau, France*
[d] *Centre de Mathématiques et de leurs Applications, UMR8536 CNRS—Ecole Normale Supérieure, 94140 Cachan, France*

Abstract

A branched geometrical structure of the mammal lungs is known to be crucial for rapid access of oxygen to blood. But an important pulmonary disease like emphysema results in partial destruction of the alveolar tissue and enlargement of the distal airspaces, which may reduce the total oxygen transfer. This effect has been intensively studied during the last decade by MRI of hyperpolarized gases like helium-3. The relation between geometry and signal attenuation remained obscure due to a lack of realistic geometrical model of the acinar morphology. In this paper, we use Monte Carlo simulations of restricted diffusion in a realistic model acinus to compute the signal attenuation in a diffusion-weighted NMR experiment. We demonstrate that this technique should be sensitive to destruction of the branched structure: partial removal of the interalveolar tissue creates loops in the tree-like acinar architecture that enhance diffusive motion and the consequent signal attenuation. The role of the local geometry and related practical applications are discussed.
© 2006 Elsevier Inc. All rights reserved.

Keywords: NMR; Restricted gas diffusion; Lung acinus model; Monte Carlo simulations

1. Introduction

Nuclear magnetic resonance (NMR) of diffusive motion in complex media is an efficient tool to probe their geometrical structure [1]. This technique has been widely used to investigate porous materials [2–6], colloidal suspensions [7], and biological tissues [8–11]. The non-invasive character of NMR appears to be particularly promising for medical applications. For instance, the use of hyperpolarized gases like helium-3 or xenon-129 for the study of human lungs gives a qualitative picture of local diseases like emphysema [12–18]. At the same time, their *quantitative* understanding still presents a challenging issue since the very complex morphology of the real acini makes

almost unfeasible any theoretical or numerical study of restricted diffusion. In this light, the choice of an appropriate geometrical model of the pulmonary acinus becomes important.

An interesting theoretical discussion was proposed by Yablonskiy et al. [19]. The signal attenuation in the lungs was approximated by an explicit relation obtained for restricted diffusion in an ensemble of isolated infinite cylinders randomly oriented in space. Strictly speaking, this was not a *geometrical* model of the acinus but rather a useful formal analogy. Actually, this "cylinder" model was based on the fact that longitudinal and transverse motions inside alveolar ducts should be significantly different. A simple theoretical relation for the NMR signal was deduced and compared to experimental measurements. Being sensitive to the diameter of the alveolar ducts, this relation was used to fit measured signals and to detect possible enlargements of these ducts, then considered as modeling of emphysema.

---

* Corresponding author. Fax: +39 81 556 75 83.
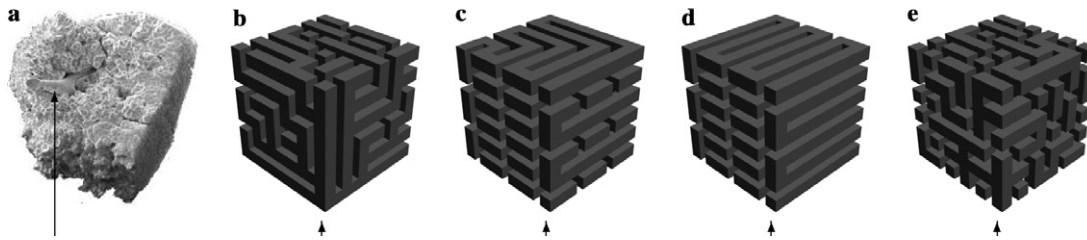*E-mail address:* denis.grebenkov@polytechnique.edu (D.S. Grebenkov).

Fig. 1. Five different geometrical structures with the same surface-to-volume ratio: (a) cast of a human acinus, (b) branched Kitaoka labyrinth, (c,d) two long channels "packed" in the cube, and (e) a disordered porous medium created by random "digging" in the cube. The first four domains satisfy the connectivity condition (accessibility from the "entry", indicated by an arrow), while the last one does not. The "solid" channels represent the volume of the confining medium where the gas diffuses.

A further numerical analysis of this model was realized by Fichele et al. [20].

Although the "cylinder" picture provides a simple interpretation, it is not satisfactory from the geometrical point of view. The alveolar ducts are very tortuous and densely fulfill a compact volume of the rib cage, providing a high surface area of the alveolar membranes within a given volume (Fig. 1a). To give a simple estimate of the surface-to-volume ratio κ, one can divide the total surface area of the human lungs (70–100 m^2) by a typical volume of around 5 l that gives $\kappa \sim 14$–20 mm^{-1} [21]. This parameter is usually assessed by stereological measurements done on lung slices [22].

A numerical study of acinus-like morphologies in 2D was recently carried out by Fichele et al. [23]. The effect of restricted diffusion was compared in three geometries: a heterogeneous porous structure, a "grape-vine" model and a "tree-like" model. It was shown that the first model did not reproduce the signal attenuation observed in the lungs. In contrast, both "grape-vine" and "tree-like" models led to similar results that could be mainly characterized by two apparent diffusion coefficients, in qualitative agreement with the "cylinder model". This work can be considered as the first numerical study of restricted diffusion in a more realistic geometry of the acinus than a cylinder or a sphere. But, at the same time, the "grape-vine" and "tree-like" models remain 2D.

The branched structure of the acinus is known to be mandatory for rapid access of oxygen to blood [24–28]. From the geometrical point of view, a tree-like structure (without loops) produces a maximum alveolar surface area under the connectivity condition: any part of the acinus should be accessible from the terminal bronchiole (i.e., the single "entry" of the acinus). Indeed, a destruction of internal "walls" would obviously decrease the surface area, while the addition of even one "wall" breaks the connectivity of the acinus. At the same time, there may exist many tree-like structures with the same surface-to-volume ratio. One example of a Kitaoka labyrinth (see below) is given in Fig. 1b. The total surface area of this labyrinth is equal to that of two realizations of a long channel filling the same cube (Fig. 1c and d). The *branched* structure is more efficient for diffusive transport when the oxygen molecules arrive from the acinar "entry".

A NMR pulsed gradient technique can be applied to monitor restricted diffusion in the human lungs in the hope to detect partial or complete destruction of the alveolar tissue. Hyperpolarized gases like helium-3 or xenon-129 are used to obtain a sufficient signal-to-noise ratio. When a patient inhales a hyperpolarized gas, its motion can be encoded by a linear magnetic field gradient. The attenuation of the macroscopic signal by diffusion can provide a useful information about the confining geometry. The aim of our work is to better understand the relation between the NMR signal attenuation and the geometry of healthy and emphysematous acini.

Emphysema is defined as "abnormal permanent enlargement of the airspaces distal to the terminal bronchioles, accompanied by destruction of their walls and without obvious fibrosis" [29]. From stereological measurements done at autopsy, a systematic decrease of the surface-to-volume ratio κ with increasing percent emphysema has been reported, with no noticeable differences between different forms of emphysema (centrilobular, panlobular, or mixed) [30]; for patients who died of lung failure due to emphysema, κ has been estimated to 67% of its value from a control group [31], with a mean κ of 14.9 mm^{-1} for the control group, and of 10.4 mm^{-1} for the emphysema patient group (with standard deviations of about 1 mm^{-1}).

In this paper, we present NMR signal attenuation computed from numerical simulations of the diffusive motion within a Kitaoka model of the acinus geometry [32]. A healthy acinus is represented as a 3D labyrinth with a dichotomic structure and non-symmetric branches of random lengths filling densely a cube as shown in Fig. 1b. Monte Carlo simulations of the translational diffusive motion have been performed to investigate how the geometrical architecture of the acinus influences the NMR signal. Partial destruction of the internal structure is also used as a model of early emphysema stages, and its effect on NMR signal attenuation is considered.

2. Physical background

Hyperpolarized gases like helium-3 or xenon-129 (with spin 1/2) have been used for MRI of the human lungs since 1990s [12–15]. After the inhalation of about 300 ml of hyperpolarized gas, the patient holds its breath for several

seconds during the NMR measurement. At ambient pressure and temperature, the gas mean free path is much shorter than the smallest geometrical feature of the acinus, so that translational motion is diffusive. Since helium atoms are almost insoluble in the blood, they do not penetrate across the alveolar membranes that can thus be seen as perfectly reflecting. In mathematical language, the translational motion of these spin-bearing particles is known as reflected Brownian motion [33,34]. The free diffusion coefficient D of helium-3 atoms is large ($D \sim 1$ cm^2/s for helium-3 in nitrogen [35]), therefore their spatial distribution becomes uniform inside the lungs at the beginning of the NMR experiment.

An application of a radio-frequency pulse flips the spin magnetizations into the transverse plane. The use of a linear magnetic field gradient in a chosen direction $\mathbf{e}$ and of effective temporal profile $gf(t)$ encodes the nuclei positions. The total phase accumulated along a trajectory $\mathbf{r}(t)$ of a diffusing nucleus until time T can be written as

$$\varphi = \gamma g \phi_{\mathbf{e}} \quad \text{where} \quad \phi_{\mathbf{e}} = \int_0^T dt\, f(t)\, (\mathbf{e} \cdot \mathbf{r}(t))$$

where γ is the nuclear gyromagnetic ratio (e.g., $\gamma = 2.037894 \times 10^8$ s^{-1} T^{-1} for helium-3), and g the maximum intensity of the gradient. In this paper, we consider a steady gradient of bipolar waveform, for which the effective profile is

$$f(t) = \begin{cases} 1, & 0 < t < T/2 \\ -1, & T/2 < t < T \end{cases} \tag{1}$$

The transverse magnetization at time T can be conveniently written in a complex form as $e^{i\varphi}$. The macroscopic NMR signal is then proportional to the average of $e^{i\varphi}$ over the whole ensemble of nuclei. Since the number of nuclei is extremely large, this average can be replaced by the expectation $\mathbb{E}$ over all possible trajectories of the reflected Brownian motion started from a randomly chosen point:

$$S_{\mathbf{e}}(g) = \mathbb{E}\{\exp[i\gamma g \phi_{\mathbf{e}}]\} \tag{2}$$

(the signal is normalized in such a way that $S_{\mathbf{e}}(0) = 1$). As a function of γg, the macroscopic signal $S_{\mathbf{e}}(g)$ appears as a characteristic function of the random variable $\phi_{\mathbf{e}}$ [36]. If the confining domain is not isotropic, the signal $S_{\mathbf{e}}(g)$ does depend on the orientation $\mathbf{e}$ of the applied gradient. The variation of the gradient direction may thus be useful to study the medium anisotropy. In some cases, however, it is convenient to average the signal over all possible gradient directions in space. If the distribution of these orientations is random, one obtains the *directionally averaged signal* as

$$S_{av}(g) = \int_{|\mathbf{e}|=1} \frac{d\mathbf{e}}{4\pi} \mathbb{E}\{\exp[i\gamma g \phi_{\mathbf{e}}]\} = \mathbb{E}\left\{\frac{\sin(\gamma g \phi)}{\gamma g \phi}\right\} \tag{3}$$

where $\phi = \sqrt{\phi_x^2 + \phi_y^2 + \phi_z^2}$.

In the case of a free unbounded diffusive motion, the signal does not depend on the gradient orientation:

$$S(g) = \exp[-D\gamma^2 g^2 T^3 / 12] \tag{4}$$

This signal would be negligible for T and g values typically used in MRI of the lungs with hyperpolarized gases ($T \sim 10$ ms, $g \sim 10$ mT/m). The presence of reflecting boundaries drastically changes the situation. Being confined by the geometry, the nuclei have to diffuse slower so that the signal decrease is not so rapid. In general, the signal is less attenuated in a smaller restrictive domain. The internal geometry also plays an important role. For two domains of the same size, a larger signal would be observed in a domain with a lower connectivity. In this light, one may expect to distinguish a healthy acinus (branched structure) and an emphysematous acinus (partially destroyed branched structure). Our aim in this paper is to understand this behavior in a quantitative way by numerical simulations.

3. Geometrical model of the acinus

The acinus as a physiological unit is not very appropriate for our study since oxygen can still be partially transported by convection at its entry. Moreover, this entry contains only a few alveoli. For this reason, it is more convenient to speak about a "sub-acinus", a 1/8 part of the acinus, where oxygen transport is purely diffusive at rest [21,24]. Throughout this paper, we shall discuss restricted diffusion in healthy or emphysematous sub-acini (and not the acinus itself). For sake of simplicity, the prefix "sub" will be generally omitted. Note that anyway the essential fraction of the gas volume lies in the very last generations of the acinar tree.

A simple model for the internal geometrical structure of the pulmonary acinus has been proposed by Kitaoka et al. [32]. The acinus is represented as a 3D labyrinth of channels with square profile (Fig. 1b). In this section, we shall describe two acinar morphologies that will be referred to as "model I" and "model II". Although their topological structures are identical as being generated by the same Kitaoka algorithm, local geometries are slightly different. We shall use this difference to check how our numerical results can be influenced, or not, by subtle geometrical details.

To illustrate the idea of the Kitaoka algorithm, let us consider an "acinus" of cubic shape that is divided into n^3 "basic cubic cells" (Fig. 2). For humans, typical dimen-
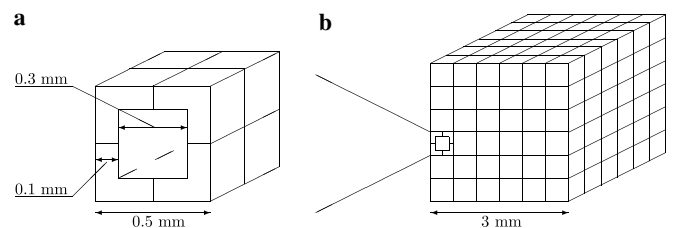

Fig. 2. Illustration of the Kitaoka model: eight alveoli form a "basic cell" of cubic shape (a); a healthy (sub)acinus is represented as 3D labyrinth composed of these "basic cells" (b).
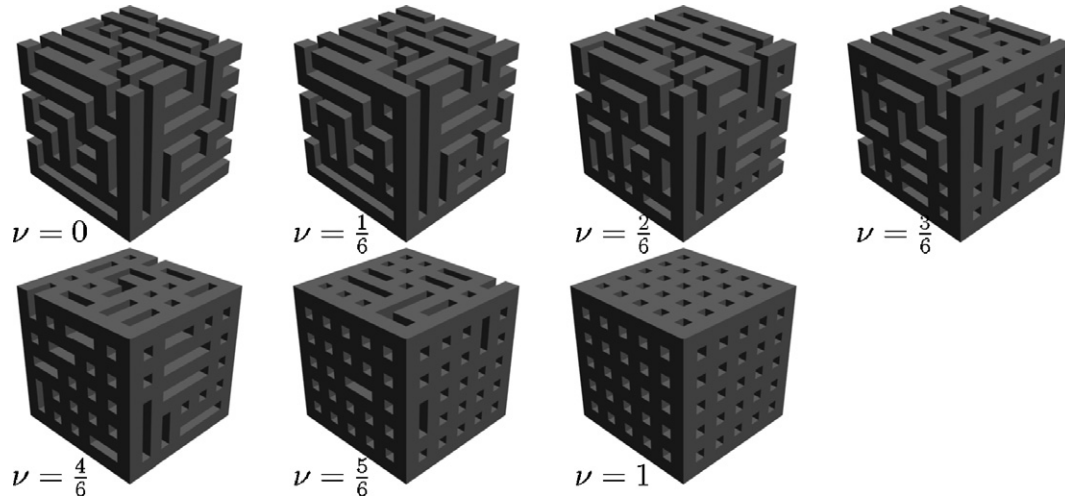
Fig. 3. Modeling of the progressive destruction of the internal alveolar tissue by emphysema. The destruction factor *v* is varied from 0 (healthy acinus) to 1.

sions for the acinus and alveolar ducts are $L \simeq 3$ mm and $\ell \simeq 0.5$ mm, respectively, whence $n = 6$. At the beginning, all basic cells are isolated from each other by intercellular walls. The Kitaoka algorithm is then used to construct the acinar labyrinth by successively destroying a part of the internal walls starting from the entry [32]. As a result, the acinus is modeled as a dichotomic branched structure filling densely the volume of the initial cubic domain (Fig. 1b). Being well appropriate for numerical simulations, this simplified geometry captures the essential features of the pulmonary acinus: a dichotomic tree with non-symmetric branches of random lengths filling the whole volume. Moreover, the total surface area and the average length of the branches correspond to those of real acini. In the two next subsections, we shall describe some geometrical features that make the Kitaoka model still more realistic. At the same time, the Kitaoka acinus remains an idealized model as compared to the real acini. In particular, the pores of Kohn between adjacent alveoli are not taken into account.

The total number of intercellular walls separating two adjacent cells is equal to $2n(n-1)$ in 2D and to $3n^2(n-1)$ in 3D. The number of intercellular walls that have been suppressed to obtain a labyrinth is equal to the number of basic cells (small cubes) minus one, that is n^2-1 in 2D and to n^3-1 in 3D. Indeed, since there is no loop in the branched structure of the labyrinth, each cell (except the "main entry") has precisely one "entry" face that has been suppressed to connect it with its adjacent cell. The number of suppressed internal walls is the same for different topological realizations of the acinus (of the same size n).

Emphysema alters the geometrical structure of the acinus. Among various pathologies [37], it can lead to a partial destruction of some intercellular walls breaking the branched structure of the pulmonary acinus. We suggest to represent emphysema in the Kitaoka model by deleting a number of randomly chosen intercellular walls. Let *v*

denote the "destruction factor", i.e., the proportion of additionally destroyed walls with respect to $3n^2(n-1)-(n^3-1)$. This number ranges from 0 for a healthy acinus to 1 for the most destroyed structure (Fig. 3). The total number of destroyed walls (i.e., the number of connections between adjacent cells) is

$$N_d = (n^3 - 1) + v(2n^3 - 3n^2 + 1) \tag{5}$$

The number of remaining intercellular walls is then

$$N_r = (1 - v)(2n^3 - 3n^2 + 1) \tag{6}$$

In our model, the external walls forming the boundary of the acinus cannot be destroyed so that their number N_e is always $6n^2$.

3.1. Model I

The geometry of the real acini is more complicated. In particular, the alveolar ducts are decorated by small and very thin alveolar membranes (septa) in order to increase the total surface area and, consequently, the efficiency of the lungs. The presence of these "obstacles" should certainly influence diffusive motion.

In the original Kitaoka model [32], the septa are represented by empty corner-like shapes with very thin barriers (Fig. 4a). The combination of eight such alveoli form a basic cell (Fig. 5 illustrates their spatial arrangement). When an intercellular wall between two adjacent cells should be destroyed to create a branched structure, only the internal square is deleted, while the septum membranes at borders are kept. Following the values suggested by Kitaoka [32], the height ℓ_s of the alveolar septum was taken of 0.1 mm. Its width (around 10 μm) is negligible with respect to other length scales of the acinus [38,39].

The Kitaoka model may seem an artificial simplification of the true acinar geometry. However, it is worth to stress that computations of the oxygen flux in that geometry has
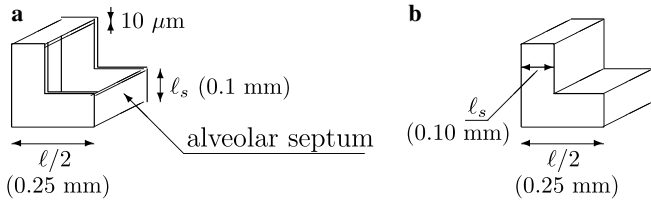
Fig. 4. The alveolus is modeled by two corner-like shapes: empty (model I, a) and thick (model II, b). In the first case, the gas can diffuse inside the corner-like shape bounded by alveolar tissue. In the second case, the corner-like shape is considered as filled by alveolar tissue forming a thick wall. If the height ℓ_s of the septum membrane was equal to 0, the two shapes would be equivalent.
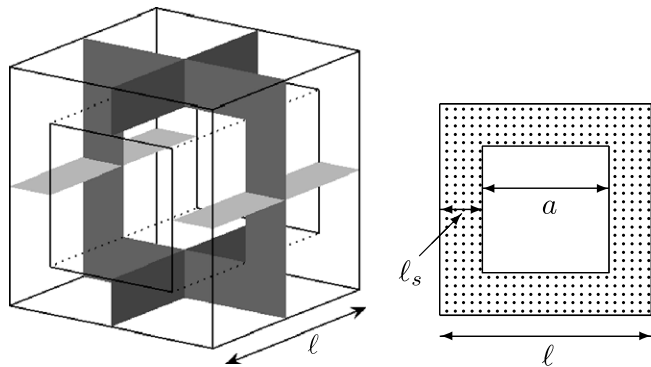

Fig. 5. Illustration of the Kitaoka basic cell formed by eight alveoli within model I. For the sake of clarity, the internal septum membranes are shown in dark gray, while the external faces are transparent (although they are formed by the same alveolar tissue). Depending on the connectivity with adjacent cells, any of the six exterior plates of the basic cell can be full (forming intercellular wall) or partially empty, with only septum at borders (allowing diffusion between adjacent cells). In the present example, the cell is connected to two adjacent cells in the direction shown by an arrow. For humans, $\ell = 0.5$ mm and $\ell_s = 0.1$ mm.

been shown to give the same results that those obtained from a renormalization technique on a real acinus [26–28].

As suggested above, emphysematous acini are modeled by a random destruction of the intercellular walls of the above healthy acinus. Wall destruction in our model would correspond to the case of panacinar emphysema. In real pathology, it is also highly probable that emphysema does create or enlarge connections between nearby acini. Since our model is limited to one sub-acinus, such complications are not taken into account. The destruction factor v, counting the proportion of destroyed walls, is directly related to the surface-to-volume ratio κ. The total surface area is

$$S_{tot} = 2 \cdot 3 \cdot 4 \cdot \ell_s^2 \cdot n^3 + 2N_r(\ell^2 + 4\ell_s(\ell - 2\ell_s))$$
$$+ 2N_d \cdot 4\ell_s(\ell - \ell_s) + \ell^2 N_e$$

The first term corresponds to internal septa, while the last term accounts the external walls. The volume is simply $n^3\ell^3$, whence one gets

$$\kappa\ell \equiv \frac{\ell S_{tot}}{V_{tot}} = 24(\ell_s/\ell)^2 + 2(1 + 4\ell_s/\ell - 8(\ell_s/\ell)^2)\frac{N_r}{n^3}$$
$$+ 8(\ell_s/\ell - (\ell_s/\ell)^2)\frac{N_d}{n^3} + \frac{6}{n} \qquad (7)$$

Since the volume does not depend on v, the normalized surface-to-volume ratio κ is a linear function of the destruction factor v. In the case of human lungs, one has $\ell \simeq 0.5$ mm, $\ell_s \simeq 0.1$ mm and $n = 6$ that leads to

$$\kappa\ell \simeq 7.69 - 2.53v \qquad (8)$$

The ratio κ varies from $7.69/\ell \simeq 15.4$ mm^{-1} for a healthy acinus to $5.16/\ell \simeq 10.3$ mm^{-1} for the most destroyed structure. The last value is still relatively high due to presence of septa. If there was no septa ($\ell_s = 0$), one would get

$$\kappa\ell = \frac{2N_r}{n^3} + \frac{6}{n} \simeq 4.01 - 3.01v$$

In this case, the limiting value $\kappa\ell = 1$ ($v = 1$) represents the surface-to-volume ratio for a cube of length $L = n\ell$ with $n = 6$.

3.2. Model II

The presence of thin septum membranes (of order of 10 μm) makes difficult or even unfeasible a practical realization of the Kitaoka acinus for experimental study. One may wonder, however, whether such subtle geometrical details would be significant or not. For instance, the numerical investigation of oxygen transfer in the Kitaoka acinus showed that septa could be taken into account by using an effective surface area [25–27]. Of course, this would be a considerable simplification of the acinar morphology for numerical and especially experimental study.

In particular, the "model II" defined below can be realized in order to build a structure constituting an experimental phantom of the Kitaoka geometry. We consider then another model of the acinus, still based on the Kitaoka labyrinth algorithm, but with "smooth" narrowed channels. The effective width a is taken to be $a = \ell - 2\ell_s$ that gives $a = 0.3$ mm for humans. In other words, the alveolus with septa is considered as a thick corner-like shape (Fig. 4b). Such representation will be referred to as "model II". Note that all pictures of the Kitaoka acini in this paper are presented in this simplified way, without drawing septa on the alveolar ducts. Differences between the two models (with the same topological structure) will be examined below, in order to clarify whether specific geometrical details are significant or not.

As previously, one can calculate the surface-to-volume ratio for model II. The total surface area is given as

$$S_{tot} = 2a^2 N_r + 8a\ell_s N_d + 6n^2 a^2$$

where the first term brings the contribution of remained intercellular walls, while the second term accounts for "passages" between connected basic cells (the last term corresponds to external walls). The total volume is

$$V = n^3 a^3 + N_d a^2 2\ell_s$$

Using the expressions (5) and (6) for N_d and N_r, one gets after a few simplifications:

$$\kappa a = 4 - \frac{4v(1-3/(2n))-2(1-v)/n^3}{1+(2\ell_s/a)-(2\ell_s/a)/n^3+2v(2\ell_s/a)[1-3/(2n)+1/(2n^3)]}$$

For $n = 6$ and $\ell_s/a = 1/3$, one has $\kappa a \simeq 4-3v/(5/3+v)$, whence $\kappa \simeq 4/a \simeq 13$ mm^{-1} for a healthy acinus ($v = 0$), and $\kappa \simeq 2.88/a \simeq 9.6$ mm^{-1} in the opposite limit $v = 1$. While the surface-to-volume ratio κ sensitively depends on the thickness $2\ell_s$ of intercellular walls (effect of septa), its topological analogue v does not. For this reason, we prefer to use this last one in order to characterize a deviation from the branched structure of the acinus.

4. Numerical technique

Translational diffusive motion of nuclei was studied here with the help of Monte Carlo simulations by home-made code implemented in C++ [40]. Once being generated by the Kitaoka algorithm, a cubic labyrinth was used to model the geometrical structure of healthy and emphysematous acini. This confining geometry was fixed during each series of Monte Carlo simulations. The diffusion coefficient D, the gyromagnetic ratio γ, the effective temporal profile $f(t)$ of the magnetic field gradient and its duration T were also fixed.

The random trajectory of the reflected Brownian motion is modeled by a sequence of n random jumps started from a randomly chosen point inside the confining domain. The number m of jumps has to be sufficiently large in order to fulfill the following conditions:

- The stochastic trajectory is composed of a large number of jumps, including a lot of reflections on the internal walls.
- The average displacement $\sqrt{2D\tau}$ along each axis during the jump duration $\tau = T/m$ is small with respect to the internal size (width) of the alveolar ducts: $\sqrt{2D\tau} \ll \ell$.

For a typical pulse gradient of duration $T \sim 10$ ms, we used $m = 1000$. This value appears large enough to model the Brownian trajectories. In particular, a further increase of m did not provide a noticeable improvement of the precision.

The starting point $\mathbf{x}_0$ is chosen randomly with a uniform distribution inside the domain. For each jump k, one generates independent Gaussian displacements $\delta\mathbf{x}^i$ in the three space directions ($i = x, y, z$) with dispersion $\sqrt{2D\tau}$, in order to pass from the current position $\mathbf{x}_k$ to a new position $\mathbf{x}_{k+1}$. If the linear segment between the current position and the new position intersects an intercellular wall or a septum membrane, a mirror reflection is applied. [1] At each jump

---

[1] Note that the mirror reflection implies that the incident angle is equal to the angle of reflection. In many physical systems, however, the angle of reflection is distributed according to the cosine law. Although this detail could be taken into account in numerical simulations, it is not significant here.

k, the term $\tau f(k\tau)\mathbf{x}_k^i$ is added to the phase counter ϕ_i for each space direction $i = x, y, z$. The total phase accumulated during the whole trajectory for unit gradient is then approximated, for each i, by the sum

$$\phi_i = \tau \sum_{k=0}^{m} f(k\tau)\mathbf{x}_k^i$$

If the gradient is applied along the direction $\mathbf{e} = (e_x, e_y, e_z)$, the total phase accumulated in this direction for unit gradient is

$$\phi_\mathbf{e} = e_x\phi_x + e_y\phi_y + e_z\phi_z$$

If one is looking for the directionally averaged signal, the averaged phase is

$$\phi = \sqrt{\phi_x^2 + \phi_y^2 + \phi_z^2}$$

Repeating the Monte Carlo simulation N times, one records this phase in order to obtain its probability distribution. Once the simulations are terminated, one can find the expectations in Eqs. (2) or (3) to obtain the signal $S_\mathbf{e}(g)$ or the directionally averaged signal $S_{av}(g)$ as a function of the gradient amplitude g.

Since the numerical computation of the expectation is based on the summation of a large number of independent realizations of the random variable ϕ, its stochastic error is of order of $1/\sqrt{N}$. The choice of $N = 10^6$ provided the results with a sufficient accuracy after 1/2 h of computation using a 2.4 GHz Intel processor. In particular, these simulations allow one to follow the signal attenuation in the range between 1 (no gradient) and 10^{-3} that is typically accessible in experiments. Being still possible, a further increase of N presents rather academic interest since experimental *in vivo* diffusion-weighted images are generally limited by a signal-to-noise ratio at most of 100.

Throughout this paper, we considered a steady gradient with a bipolar temporal profile (1), with infinite slew rate. The free diffusion coefficient D of helium-3 was fixed to be 1 cm^2/s, which corresponds to a typical helium-3/nitrogen gas mixture (for pure helium-3, $D \simeq 2$ cm^2/s). The total gradient duration T and intensity g were varied in ranges between 1–100 ms and 0–50 mT/m, respectively, that essentially cover experimental values feasible in modern medical MR scanners.

The Monte Carlo simulations have been tested on several cubic-like domains. For this purpose, the signal has been independently calculated by means of the multiple correlation function approach [34]. This technique issued from the matrix formalisms [41–43] gives very accurate results for the domains, for which the Laplace operator eigenbasis is known explicitly (e.g., a cube). These tests showed that the Monte Carlo simulations were accurate when the signal amplitude was larger than 10^{-3} as expected.

5. Results

Before starting the numerical analysis, it is worth estimating what kind of restricted diffusion can be expected.

For a typical value $T = 10$ ms, the characteristic diffusion length $\sqrt{DT}$ is 1 mm. That means that nuclei explore on average one or two basic cells (of size 0.5 mm). This is an *intermediate* situation between slow and fast diffusion regimes. On the one hand, nuclei diffuse far enough to "feel" the presence of restrictive boundaries and to probe a connection between adjacent basic cells. In this sense, the branched structure of the acinus should be already relevant. On the other hand, nuclei have no time to travel over the whole acinar morphology. One should not then expect that the whole topological branching structure can be revealed in detail. One will see that this qualitative reasoning is in fact correct. The main question to be addressed in the following subsections is to know how the geometrical structure of the acinus does influence signal attenuation.

5.1. Different random realizations of a healthy acinus

The Kitaoka algorithm presents the advantage that different random structures of a healthy acinus can be generated (see Fig. 6). This feature allows one to reproduce a physiological variety of real acini. Since each realization of the acinus has its proper geometry, one may wonder whether signal attenuation would be different from one morphology to another.

To check this point, we first applied a linear magnetic field gradient of duration $T = 10$ ms along the x axis. The signal $S_x(g)$ as a function of the gradient amplitude g is shown in Fig. 7 for different realizations of the healthy acinus. As one can expect, these curves present large deviations from each other. Which curve should be taken to be compared, for example, to experimental data? Should one average the signal over different random realizations? What such an average would mean? Trying to answer these questions would lead us to a study of specific combinatorial problems related to the Kitaoka algorithm. Even if such a study was undertaken, its results would merely correspond to this particular model and could be quite disconnected from the behavior in human lungs.

Fortunately, nature provides a simple and elegant solution to this problem. It is based on the fact that the real acini are *randomly* oriented in the chest. Consequently, the signal measured in the lungs with a fixed gradient direction is already averaged over all possible orientations of the acini. This is equivalent to an abstract situation in which all acini would be aligned along the same direction, but the gradient orientation would be random in space. In other
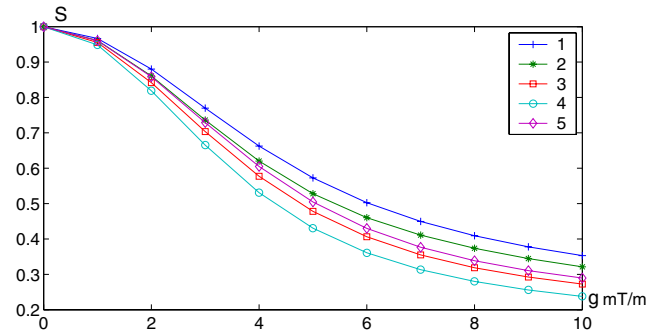

Fig. 7. Signal $S_x(g)$ as a function of the gradient amplitude g for different realizations of the healthy acinus (model I) shown in Fig 6. The gradient is oriented along axis x. A similar large deviation was observed for model II (not presented).

words, experimental data for real lungs should be compared to the *directionally* averaged signal $S_{av}(g)$, and not to the signal with a fixed gradient direction.

The situation is drastically changed when one considers the signal averaged over all possible gradient directions in space. As shown in Fig. 8, the signal dependences on the gradient amplitude for all realizations of the healthy acinus collapsed onto a single curve. It is thus sufficient to consider a single realization of the healthy acinus and compute the directionally averaged signal $S_{av}(g)$ to obtain a representative behavior. All data further presented have been obtained in this way.
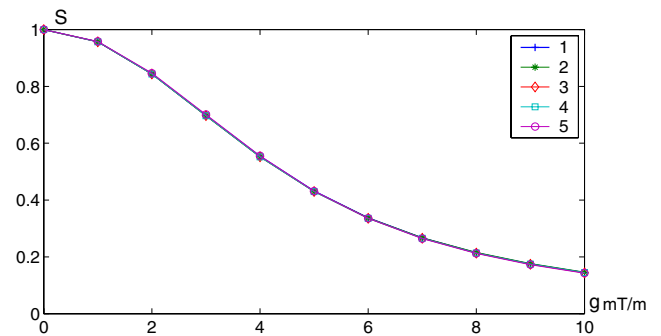

Fig. 8. Directionally averaged signal $S_{av}(g)$ as a function of the gradient amplitude g for different realizations of the healthy acinus (model I) shown in Fig 6. All data collapsed onto the same curve independently of a particular realization of the healthy acinus. A similar collapse was observed for model II (not presented).
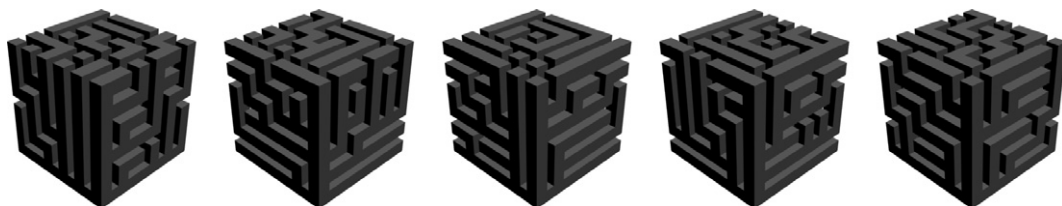

Fig. 6. Five random realizations of a healthy acinus.

5.2. Comparison between healthy and emphysematous acini

The signal found for a healthy acinus model was first compared to that for an emphysematous model. As described in Section 3, the deviation from the healthy branched structure is characterized by the destruction factor v. To model different stages of emphysema, this factor can be ranged from 0 (healthy acinus) to 1. Starting from a chosen realization of the healthy acinus, one randomly removed $v[3n^2(n-1) - (n^3-1)]$ intercellular walls. By construction, the obtained geometry for the emphysematous acinus was also random.

Fig. 9 shows the directionally averaged signal $S_{av}(g)$ as a function of g for emphysematous acini with different v. As for the healthy acinus, different random realizations of the emphysematous acinus with the same v value led to the same signal $S_{av}(g)$. In contrast, the curves corresponding to emphysematous acini with different v were well distinguishable. The difference between the original branched structure and the partially destroyed one was sharper for higher gradient intensity g. In fact, one obtains an apparent exponential decrease of the directionally averaged signal as a function of the destruction factor v at fixed gradient intensity:

$$S_{av}(g,v) \simeq S_{av}(g, v=0) \exp[-A(g)v] \qquad (9)$$

Here the coefficient $A(g)$ is a function of the gradient intensity. Fig. 10 shows a very good agreement between the dependence of the signal $S_{av}(g,v)$ on v and its exponential fit for $g = 5\,\text{mT/m}$ and $g = 10\,\text{mT/m}$ (here $A \simeq 1.96$ and 3.46, respectively). At higher g, the coefficient $A(g)$ was bigger so that partial destruction of the alveolar tissue led to sharper attenuation of the signal. Consequently, one expects that a MRI diagnosis of emphysema would be more sensitive at higher gradients.

The gradient intensity achievable in practical situations is of course limited. Among different reasons, one can mention hardware limitation and medical precautions. In turn, a relatively small signal-to-noise ratio for *in vivo* measurements makes difficult an accurate treatment of small NMR signals obtained at high gradients. One may thus wonder which gradient intensity would be the optimal one. Such intensity would depend on the particular sequence, timing parameters and experimental conditions (e.g., signal-to-noise ratio). To get the idea of such an optimal intensity, the coefficient $A(g)$ was investigated as a function of g. Fig. 11 shows that this coefficient grew sharply at the beginning ($g \leqslant 10\,\text{mT/m}$), but then this increase slowed down at $g \geqslant 10\,\text{mT/m}$. Consequently, there should be no need to use very high gradients (say, larger than $20\,\text{mT/m}$ in our example) to make the MRI technique more sensitive to partial destruction of the alveolar tissue. This observation may be useful to improve medical diagnosis of emphysema at early stages. We have to stress, however, that the given gradient values are specific of our choice of sequence and timing parameters.

The signal decrease as a function of v is not surprising. It is simply related to the fact that diffusion becomes more rapid in a partially destroyed structure that leads to faster dephasing. In particular, the presence of the pores of Kohn between alveoli in real acini may lead to a slightly stronger signal attenuation. In contrast, the *exponential* decrease appears as an intriguing empirical result. It means that the logarithm of the directionally averaged signal is a linear function of the destruction factor v and, using (8), of the surface-to-volume ratio κ. The signal attenuation can thus
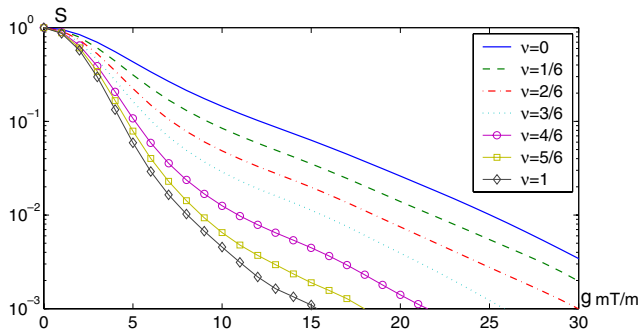

Fig. 9. Directionally averaged signal $S_{av}(g)$ as a function of g for different destruction factors v starting from 0 (healthy acinus) and ranging up to 1 to model different emphysematous acini. Note that the functional form of these curves would depend on the timing parameters for the diffusion sensitizing gradient profile.
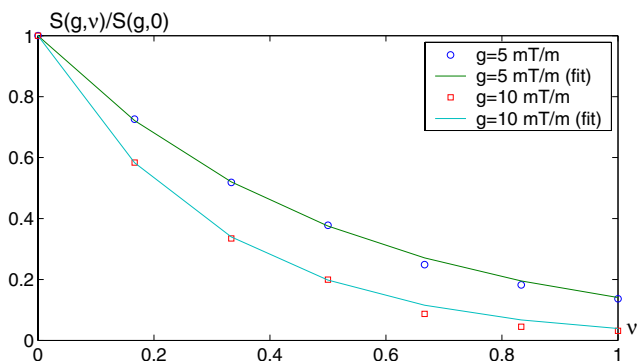

Fig. 10. Ratio $S_{av}(g,v)/S_{av}(g, v=0)$ as a function of the destruction factor v and its exponential fit for two values of the gradient intensity g.
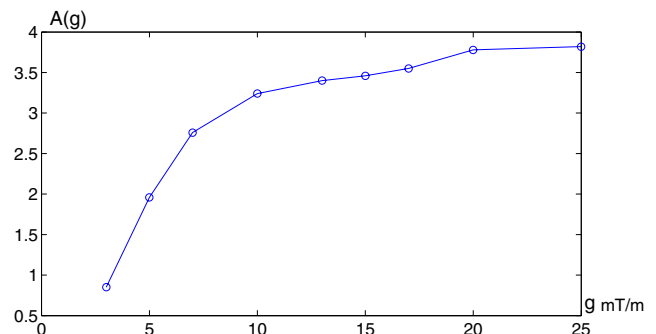

Fig. 11. Coefficient A as a function of g. The increase of the gradient intensity g led to a sharper dependence of the signal $S_{av}(g,v)$ as a function of v. However, a saturation effect was present at relatively high gradients.

be seen as a linear measure of the partial destruction of the alveolar tissue. It is worth to note that a linear dependence of ln $S(g)$ on the surface-to-volume ratio κ is known to be a characteristic feature of slow diffusion in porous media [3]. Our case is rather different since the diffusion length $\sqrt{DT} \simeq 1$ mm is larger than the inner diameter of the alveolar ducts (0.3 mm). In the next subsection, the role of the surface-to-volume ratio will be investigated from another point of view.

5.3. Destruction of septum membranes

The essential advantage of the Kitaoka labyrinths with respect to other geometrical models is that they reflect the branched structure of the acinus. In previous subsection, we have seen how a partial destruction of this structure could influence signal attenuation. However, emphysema can damage not only the intercellular walls but also the septum membranes inside each basic cell. One may thus wonder how this particular destruction would change the signal. Fig. 12 presents signal attenuation for model healthy acini with different septum heights: $\ell_s = 0.1$ mm (normal septa), $\ell_s = 0.05$ mm (reduced septa) and $\ell_s = 0$ (no septa). Results for model emphysematous acini with normal septa are also shown for comparison. Results with reduced septa were close to those of the healthy acinus with normal septa. With no septum at all, the deviation became more pronounced. But note that the destruction of all septum membranes had a much weaker impact on restricted diffusion and the consequent signal attenuation than a partial destruction of the branched structure with $v = 2/3$.

To complete this analysis, let us compare the surface-to-volume ratios κ for different cases. Using relation (7), one finds 15.4, 11.9, and 8.0 mm^{-1} for $\ell_s = 0.1$ mm (normal septa), $\ell_s = 0.05$ mm (reduced septa) and $\ell_s = 0$ (no septa), respectively. These ratios for $v = 1/6$ and 4/6 are 14.5 and 12.1 mm^{-1}, respectively. Such changes of κ are representative of changes found in patients who died due to emphysema as compared to controls [31], except for the very small κ value found for model I without septa. The knowledge of κ makes the above observation more striking. Indeed, decreasing the septum height by one half reduced the surface-to-volume ratio (from 15.4 to 11.9 mm^{-1}), while the signal attenuation was almost not changed. On the contrary, a similar decrease of the surface-to-volume ratio by destruction of the branched structure (from $v = 0$ to 4/6) led to a considerable signal attenuation. Such an effect should be detectable in the hardware conditions of medical MR scanners. The above comparative analysis of signal attenuation between structures of similar κ values but with different topological architectures clearly reveals the significance of the acinar branched structure and its impact on restricted diffusion.

5.4. Apparent diffusion coefficient

Signal attenuation by restricted diffusion in porous media is frequently characterized by an apparent diffusion coefficient (ADC). And this notion is widely used in diffusion-weighted MRI of the lungs with hyperpolarized gases. Multiple reflections from the alveolar tissue slow down the diffusive propagation of nuclei. Under certain conditions, this motion can be approximated as free diffusion with a smaller diffusion coefficient (ADC). In this case, the expression (4) for signal attenuation can be written in a simple form

$$S = \exp[-b\ \text{ADC}] \tag{10}$$

where the coefficient

$$b = \gamma^2 g^2 T^3 / 12 \tag{11}$$

combines different characteristics of the applied gradient (intensity, duration and effective temporal profile). This relation suggests that ln S plotted against b should appear as a straight line. An ADC measure can then be obtained from a standard non linear fit of experimental data to Eq. (10). For unrestricted diffusion, one gets ADC = D.

In spite of its common applications, Eq. (10) remains an approximation which *may or may not* be valid. It is always applicable for small b, but is known to be invalid, at least in
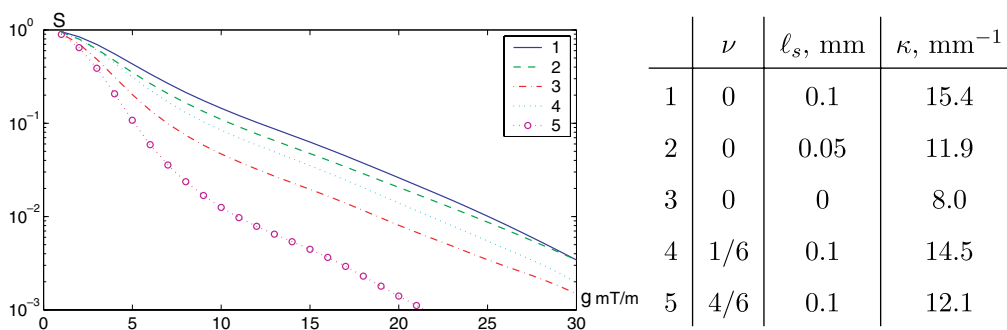

	ν	ℓ_s, mm	κ, mm^{-1}
1	0	0.1	15.4
2	0	0.05	11.9
3	0	0	8.0
4	1/6	0.1	14.5
5	4/6	0.1	12.1

Fig. 12. Role of the septum membrane on signal attenuation. Partial ($\ell_s = 0.05$ mm) or total ($\ell_s = 0$) destruction of septa led to faster signal attenuation. Total destruction of septa had a stronger impact than a partial destruction of the branched structure with $v = 1/6$ but a much weaker one than that with $v = 4/6$.
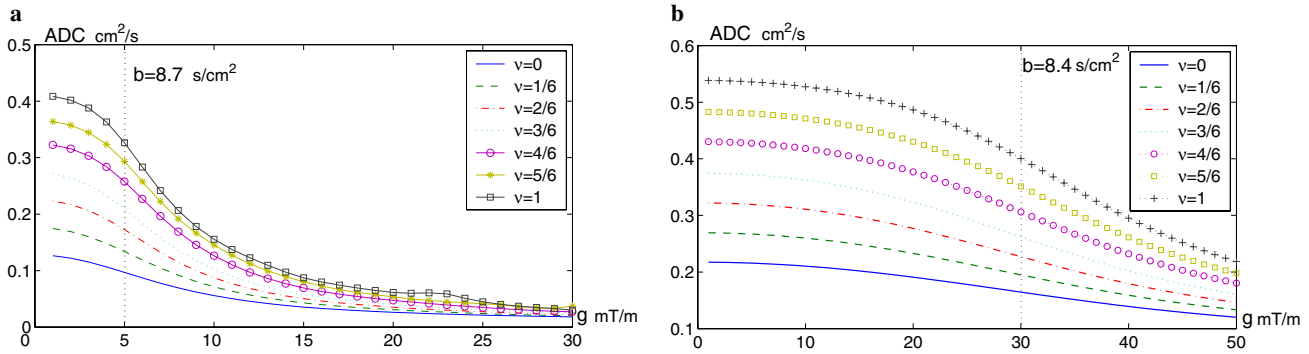
Fig. 13. Apparent diffusion coefficients for healthy and emphysematous acini. Most experimental measurements of the ADC in the lungs were realized for relatively small b. Left: $T = 10$ ms; right: $T = 3$ ms.

certain cases, for relatively large b. The related discussion is out of the scope of the present paper (for further information, see [34] and references therein).

To check the validity of relation (10) for our data on model healthy and emphysematous acini, one can plot ADC $= -\ln S/b$ as a function of b. If this coefficient was a characteristic of the alveolar tissue, it should not depend on b. Fig. 13 reveals a very different behavior. For all studied acinar structures, ADC decreased with b (or g). Strictly speaking, these ADCs have no meaning as *diffusion coefficients*, and can only be used as a notation for the ratio $-\ln S/b$. The ADC dependence on b is a sign of a non-Gaussian behavior. However, the related signal attenuation is still dominated by an exponential g^2 dependence, with a certain prefactor depending on g. Moreover, the dependence of the ADC on b (or g) can be formally interpreted as a transition between two Gaussian regimes, as suggested by Yablonskiy et al. within the "cylinder model" [19]. This observation is related to the fact that the spins diffusing during time T (here 10 ms) explore distances of order of the size of the alveolar ducts. In other words, these spins behave as if they could mainly "feel" the presence of the ducts, but not their branching structure. Note, however, that the "cylinder model" contains three fitting parameters that makes it automatically more adjustable than a simple Gaussian form. When this model was used to fit our numerical data for a healthy acinus at $T = 10$ ms, the longitudinal and transverse diffusion coefficients D_L and D_T took values 0.39 and 0.014 cm^2/s, respectively. The first value is in agreement with experimental data reported in [19]. The second value is one order of magnitude smaller. This can be attributed to the motional averaging character of restricted diffusion. Indeed, in this regime, the signal attenuation and the transverse diffusion coefficient are very sensitive to the characteristic size of the confining domain: $D_T \propto a^4$ [44,45]. In our simulation, the alveolar size a was taken of 0.5 mm, while its value was of about 0.75 mm in [19], whence one gets $(0.75/0.5)^4 \simeq 5.06$, which explains the difference. Note also that modeling of the alveolar duct geometry by cylinders or by square profile channels is another source of difference. We conclude that the "cylin-

der model" seems to be applicable to fit our numerical data for model I, at least for moderate b-values. Another empirical fitting function might be a linear combination of two or more Gaussians as suggested in a recent experimental study by Shanbhag et al. [17].

It is worth to remind that most ADC measurements in the lungs were realized for relatively small b-values. In this case, the approximation (10) may still be valid, giving a more or less constant ADC value (see narrow plateau for small b in Fig. 13). However, even in this case, it may be difficult to know whether a large dispersion of the measured ADC values results from geometrical features of the lungs or from non-Gaussian attenuation of the signal. In any case, the ADC determination as the ratio $-\ln S/b$ within a single measurement of the signal at one b-value may be misleading. At least a few measurements with different b-values are required to check that the Gaussian relation (10) holds. If this is the case, ADC can be found from $S(b)$ by standard nonlinear fit.

Finally, we outline a progressive increase of ADC (at small b) with the destruction factor v, as expected. The ADC values shown in Fig. 13 are in a good qualitative agreement with experimental findings reported in the literature [13–19] for healthy non smoking subjects, healthy smoking subjects or emphysematous patients.

5.5. Comparison between model I and model II

The numerical results presented in the previous subsections were obtained for model I. We also checked how the above results would be influenced by specific geometrical details of the basic cell. To this purpose, signal attenuations were compared between model I and model II. We remind that these models exhibit the same topological (branched) structure but different local geometries of the basic cell. Fig. 14 shows the directionally averaged signal as a function of g for both cases. When the gradient intensity was relatively small ($g \leqslant 10$ mT/m), signal attenuation for both models was essentially the same. In fact, the characteristic dephasing length can be estimated for $g = 10$ mT/m and $T = 10$ ms as $2\pi/(\gamma g \ T) \simeq 0.3$ mm
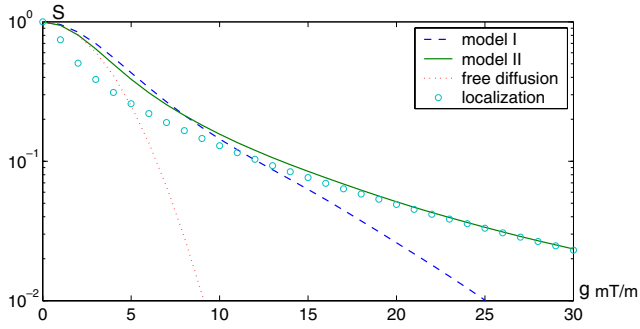
Fig. 14. Comparison between model I and model II. For a small gradient intensity ($g \leqslant 10$ mT/m), signal attenuation for both models was essentially the same. When g exceeds 10 mT/m, one can see a drastic deviation: data for model I still followed a Gaussian-like g^2-dependence, while data for model II exhibited a strongly non-Gaussian behavior, known as the localization regime. A Gaussian signal attenuation with ADC = 0.16 cm²/s is also shown for comparison.

that corresponds to the inner diameter of the alveolar ducts. It is then expected that for smaller gradients one examines larger distances. However, when g exceeded 10 mT/m, the details of the basic cell became significant, and a drastic deviation appeared between the two models. As we have already seen, signal attenuation within model I was mainly determined by a g^2-dependence, with some gradient-dependent prefactors. In contrast, model II exhibited a strongly non-Gaussian behavior. A more careful analysis of the solid curve in Fig. 14 revealed a $g^{2/3}$-dependence of ln S as a function of g. This is a characteristic feature of the localization regime [47–49]. When the gradient intensity is relatively high, nuclei diffusing in the bulk are completely dephased so that their contributions to the signal become negligible. However, nuclei diffusing near boundaries are more confined and less mobile. Consequently, their dephasing is not as pronounced, and the signal decreases slower than for nuclei in the bulk, producing a $g^{2/3}$ dependence instead of a g^2 one. The localization regime was first theoretically predicted by Stoller et al. [47] and then experimentally observed by Hürlimann et al. [49]. Using the b-coefficient defined in (11), the signal attenuation can be written as

$$S \simeq (bD)^{-1/6} \exp[-\alpha(bD)^{1/3} - \beta] \qquad (12)$$

where α and β are numerical coefficients, and D is the free diffusion coefficient. This theoretical relation was obtained by Stoller et al. for 1D restricted diffusion and then argued by de Swiet and Sen to be applicable to describe the localization regime in any geometry [48]. This relation was applied to fit the signal attenuation of our numerical results with model II. As seen in Fig. 14, a good agreement was obtained for $g \geqslant 15$ mT/m with $\alpha = 0.385$ and $\beta = 0.2$ [46].

We conclude that the model II, introduced as a potential simplification of the acinar morphology with septa (model I), can be effectively used only for relatively small gradients (in the above example, for $g \leqslant 10$ mT/m). For higher intensities, however, both models lead to very different behaviors.

Note that model II can be used to build an experimental phantom with which a more complete set of experiments could be realized in various types of NMR scanners allowing to explore a wide range of time and gradient scales.

5.6. Modeling of the acinus by porous media

The irregular geometry of the lungs can be thought of at first glance as a disordered porous medium. But the acinus has a specific 3D branching. One can question whether such a simplification gives a representative model of a real acinus. In order to check whether branching had specific consequences on signal attenuation, we examined a number of different disordered structures, all generated from a cube composed of n^3 smaller cubes, similarly to the starting point of the Kitaoka labyrinth. Then a fixed number N_d of intercellular walls were suppressed at random. We remind that this number is related to the destruction factor v by Eq. (5). For example, one had to suppress 215 intercellular walls to obtain the disordered structure shown in Fig. 1e, with the same surface-to-volume ratio κ as that of our model healthy acinus. Fig. 15 helps to compare signal attenuation in branched structures (healthy and emphysematous acini) and in disordered media. In both cases, a progressive destruction of intercellular walls enhanced the attenuation. However, signals in disordered media were systematically larger than those in branched structures (for the same gradient intensity). This observation is relat-

	type	v	κ, mm^{-1}
1	B	0	15.4
4	R		
2	B	1/6	14.5
5	R		
3	B	1/3	13.7
6	R		
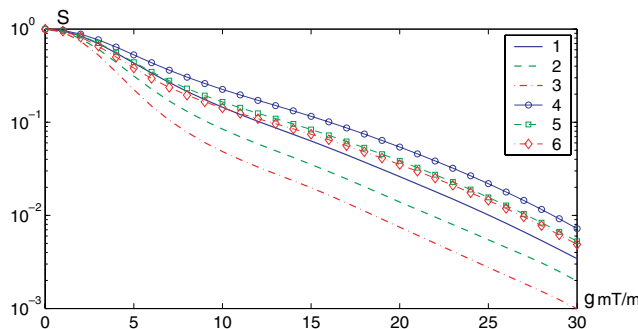
Fig. 15. Comparison of signal attenuation in branched (B) and disordered random (R) structures of the same surface-to-volume ratio.
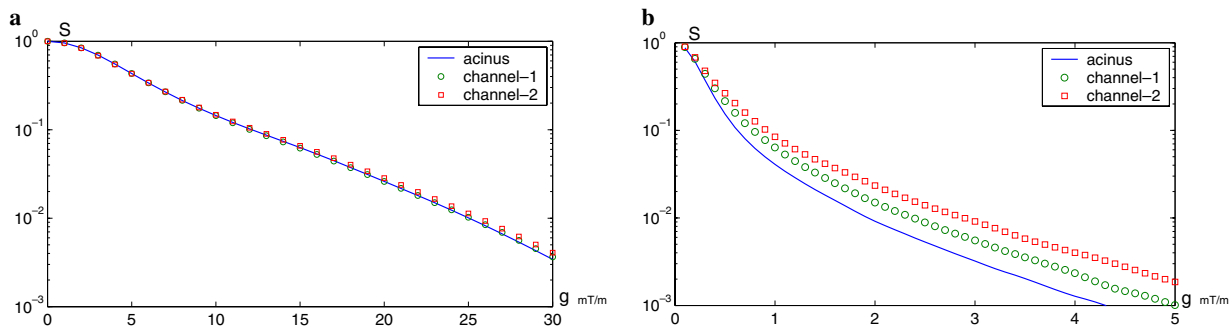
Fig. 16. Comparison of signal attenuation in a healthy model acinus and in two long channels filling the same volume (see Fig. 1b–d). The data on the left ($T = 10$ ms) fall onto the same curve since diffusing particles have no time to explore the structure. By contrast, the data on the right ($T = 100$ ms) are well distinguishable.

ed to the fact that there is a lot of isolated cells or groups of cells in disordered media. Diffusion therein is much more restricted and signal attenuation is then less pronounced. We conclude that modeling the acinus by isotropic porous media may be misleading. The branched structure of the lungs is an important feature that should be taken into account.

5.7. Branched structure of the acinus?

We would like to end this section by repeating the same question which we started with: "How the branching structure of the acinus does influence the signal attenuation?". The answer to this question could be a key to diagnose partial destruction of the lungs by emphysema at early stages. In previous subsections, we have seen that a progressive destruction of intercellular walls led to faster diffusion and could be detected as a more pronounced signal attenuation. The NMR measurement was shown to be more sensitive to destruction of the branched structure than to reduction of the septum membranes. There is no doubt now that the branched structure is important. But what kind of branching is really significant? Is the signal sensitive to the average length of branches, or to the dichotomic structure of the acinus? Can one determine the topological structure of the acinus by measuring directionally averaged signal?

A convincing answer to these questions is given by Fig. 16 where the signal attenuation is compared in a healthy acinus and in two long channels filling the same volume (Fig. 1b–d). We remind that these three structures have the same surface-to-volume ratio. Formally speaking, all these structures are branched in the sense that there are no loops. In the case of long channels, the branching is of course trivial (there is only one very long branch). Fig. 16(a) shows that the signal attenuation was almost identical for these three morphologies for a typical sequence time $T = 10$ ms. That means that the NMR measurement cannot distinguish the topological structure of the acinus. On the one hand, this behavior results from the directional averaging of the signal. If one considered

the gradient with a fixed direction, the signal would be certainly different. However, as we mentioned earlier, directional averaging is a natural and mandatory procedure to compare numerical and experimental data. On the other hand, this behavior is related to the fact that the diffusion length $\sqrt{DT} \simeq 1$ mm is of order of the size of the alveolar ducts. As a consequence, the spins diffusing during time T can explore a few basic cells. Figuratively speaking, they do not "see" the dichotomic branching of the acinus. If one could considerably increase the sequence time T, the difference between the acinus and two channels would be measurable (see Fig. 16b). A few studies have explored this possibility using stimulated echoes [50,51]. In medical applications, however, one tries to reduce T to avoid artifacts from physiological movements (such as heart beats) and to acquire the largest possible amount of data during one breath hold.

On the other hand, small animals like mice have smaller alveolar ducts than humans [24,52]. Therefore, at similar time scales T, the influence of the dichotomic acinus branching might be revealed. It will thus be interesting to perform studies with such small animal models. This is also true for experimental phantoms of model II.

We can conclude that what appears really important to diagnose emphysema by diffusion-weighted NMR is a creation of loops in the branched structure of a healthy acinus. These loops considerably speed up diffusion and can thus be detected by a more pronounced signal attenuation.

6. Conclusions

In this paper, the problem of restricted diffusion in the lungs has been numerically investigated. The main emphasis has been placed on the role of the branched structure of the acinus to signal attenuation by diffusion. The internal geometry of the acinus has been modeled by 3D dichotomic labyrinths filling a given volume. Our approach is thus the first one which takes into account the specific topology of lung parenchyma and evaluates its influence on the NMR signal attenuation. These structures have been randomly generated by the Kitaoka algorithm. The septum

membranes have been treated either explicitly (model I), or as an effective narrowing of alveolar ducts (model II). A degradation of the alveolar tissue by emphysema has been modeled as a destruction of a fixed number of intercellular walls between randomly chosen adjacent basic cells. Although our model cannot aim to take into account details of the various pathological forms of pulmonary emphysema, it allowed us to demonstrate important differences due to subtle geometrical or architectural changes.

A number of original numerical results have been reported. When partial destruction of the alveolar tissue creates loops in the branched structure, diffusion becomes faster, and the signal is then more attenuated. The high sensitivity of NMR to this effect could be used to diagnose emphysema at early stages. In particular, the logarithm of the signal appeared to be a linear function of the destruction factor v. The related coefficient $A(g)$ sharply increased with the gradient intensity g when $g \leqslant 10$ mT/m. The sensitivity of NMR can thus be improved by using higher gradients. At the same time, a saturation of the dependence $A(g)$ versus g has been observed, which means that there is no need to use very high gradients. The optimal intensity may depend on the effective gradient profile, its duration and other experimental conditions.

The role of the surface-to-volume ratio κ has been studied. We have shown that a partial or complete destruction of the septum membranes creates a drastic decrease of κ, but the signal attenuation can be less pronounced. On the contrary, a partial destruction of the branched structure leads to a moderate κ reduction, but the signal is more attenuated. We interpret such a different behavior as the fact that the destruction of intercellular walls allows adjacent cells to exchange diffusing nuclei, which speeds up their dephasing much more efficiently than a destruction of the septum membranes.

When the gradient is relatively small, the signal attenuation has almost no dependence on the specific geometry of basic cells. The numerical simulations in geometrical models I and II gave similar results. For higher gradients, however, the two models exhibit a very different behavior. The signal attenuation within model I could be qualitatively understood as a transition between two Gaussian regimes with different ADCs. In contrast, model II showed a strongly non-Gaussian behavior similar to that of a localization regime. This observation has three practical consequences. On the one hand, the numerical results, being independent of a particular geometry of the basic cell at small gradients, are likely to be valid for real acini. On the other hand, high gradients would enhance specific features of the acinus. Such measurements could thus be more sensitive to the acinar structure. At last, the simpler model II cannot replace the model I if the gradients are intense.

For experimental validation of the reported results, restricted diffusion of hyperpolarized helium-3 has been recently studied in a tenfold scale phantom of a healthy Kitaoka acinus (model II) made of epoxy resin [53]. Fur-

ther measurements with animal models will be compared to simulated data and to measurements on the phantom. A thorough comparison to experimental data on healthy and emphysematous subjects will reveal whether the Kitaoka model is sufficient to quantitatively predict the signal attenuation in the real lungs. It should be stressed, however, that experimental limitations (signal-to-noise ratio, waveform duration, gradient intensity) may make difficult a complete exploration of the specific features of the branched structure. Another important issue for future research would be development of a more realistic geometrical model of emphysematous acini. Such a model should take into account not only partial destruction of the alveolar membranes, but also possible enlargement of the alveoli and alveolar ducts at early emphysema stages.

Finally, we have seen that the NMR measurement is sensitive to the creation of loops in the branched structure, but it cannot practically help to detect the topology of branching. In particular, the signal attenuation was almost identical in the healthy acinus model and in long channels filling the volume with the same surface-to-volume ratio. Future work should consider how simple medical protocols could be deduced from such results, and how the time sequences of the pulse gradient could improve the sensitivity of the measurements in terms of specific acinar geometric modifications.

References

[1] P.T. Callaghan, Principles of Nuclear Magnetic Resonance Microscopy, Clarendon Press, Oxford, 1991.

[2] P.T. Callaghan, A. Coy, D. MacGowan, K.J. Packer, F.O. Zelaya, Diffraction-like effects in NMR diffusion studies of fluids in porous solids, Nature 351 (1991) 467.

[3] P.P. Mitra, P.N. Sen, L.M. Schwartz, P. Le Doussal, Diffusion propagator as a probe of the structure of porous media, Phys. Rev. Lett. 68 (1992) 3555.

[4] D.J. Bergman, K.-J. Dunn, Theory of diffusion in a porous-medium with applications to pulsed-field gradient NMR, Phys. Rev. B 50 (1994) 9153.

[5] M.D. Hürlimann, K.G. Helmer, L.L. Latour, C.H. Sotak, Restricted diffusion in sedimentary rocks. Determination of surface-area-to-volume ratio and surface relaxivity, J. Magn. Reson. A 111 (1994) 169.

[6] Y.-Q. Song, S. Ryu, P.N. Sen, Determining multiple length scales in rocks, Nature (London) 406 (2000) 178.

[7] B. Balinov, P. Linse, O. Söderman, Diffusion of the dispersed phase in a highly concentrated emulsion: emulsion structure and film permeation, J. Coll. Int. Sci. 182 (1996) 539.

[8] K.R. Brownstein, C.E. Tarr, Importance of classical diffusion in NMR studies of water in biological cells, Phys. Rev. A 19 (1979) 2446.

[9] W.S. Price, P.W. Kuchel, Restricted diffusion of bicarbonate and hypophosphite ions modulated by transport in suspensions of red blood cell, J. Magn. Reson. 90 (1990) 100.

[10] S.R. Wassall, Pulsed field gradient-spin echo NMR studies of water diffusion in a phospholipid model membrane, Biophys. J. 71 (1996) 2724.

[11] P.W. Kuchel, A. Coy, P. Stilbs, NMR "diffusion-diffraction" of water revealing alignment of erythrocytes in a magnetic field and their dimensions and membrane transport characteristics, Magn. Reson. Med. 37 (1997) 637.

[12] M.S. Albert, G.D. Cates, B. Driehuys, W. Happer, B. Saam, C.S. Springer Jr., A. Wishnia, Biological magnetic resonance imaging using laser-polarized 129-Xe, Nature 370 (1994) 199.

[13] B.T. Saam, D.A. Yablonskiy, V.D. Kodibagkar, J.C. Leawoods, D.S. Gierada, J.D. Cooper, S.S. Lefrak, M.S. Conradi, MR imaging of diffusion of 3He gas in healthy and diseased lungs, Magn. Reson. Med. 44 (2000) 174.

[14] H.E. Moller, X.J. Chen, B. Saam, K.D. Hagspiel, G.A. Johnson, T.A. Altes, E.E. de Lange, H.-U. Kauczor, MRI of the lungs using hyperpolarized noble gases, Magn. Reson. Med. 47 (2002) 1029.

[15] E.J.R. van Beek, J.M. Wild, H.-U. Kauczor, W. Schreiber, J.P. Mugler, E.E. de Lange, Functional MRI of the lung using hyperpolarized 3-Helium gas, J. Magn. Reson. Imaging 20 (2004) 540.

[16] A.J. Swift, J.M. Wild, S. Fichele, N. Woodhouse, S. Fleming, J. Waterhouse, R.A. Lawson, M.N.J. Paley, E.J.R. van Beek, Emphysematous changes and normal variation in smokers and COPD patients using diffusion 3He MRI, Eur. J. Radiol. 54 (2005) 352.

[17] D.D. Shanbhag, T.A. Altes, G.W. Miller, J.F. Mata, J. Knight-Scott, q-space analysis of lung morphometry *in vivo* with hyperpolarized 3He spectroscopy, J. Magn. Reson. Imaging 24 (2006) 84–94.

[18] S.B. Fain, S.R. Panth, M.D. Evans, A.L. Wentland, J.H. Holmes, F.R. Korosec, M.J. O'Brien, H. Fountaine, T.M. Grist, Early emphysematous changes in asymptomatic smokers: detection with 3He MR imaging, Radiology 239 (2006) 875–883.

[19] D.A. Yablonskiy, A.L. Sukstanskii, J.C. Leawoods, D.S. Gierada, G.L. Bretthorst, S.S. Lefrak, J.D. Cooper, M.S. Conradi, Quantitative *in vivo* assessment of lung microstructure at the alveolar level with hyperpolarized 3He diffusion MRI, PNAS 99 (2002) 3111.

[20] S. Fichele, M.N.J. Paley, N. Woodhouse, P.D. Griffiths, E.J.R. van Beek, J.M. Wild, Finite-difference simulations of 3He diffusion in 3D alveolar ducts: comparison with the "cylinder model", Magn. Reson. Med. 52 (2004) 917.

[21] E.R. Weibel, The Pathway for Oxygen. Structure and Function in the Mammalian Respiratory System, Harvard University Press, Cambridge, Massachusetts and London, England, 1984.

[22] E. Weibel, Morphometry of the Human Lung, Academic Press, New York, 1963.

[23] S. Fichele, M.N.J. Paley, N. Woodhouse, P.D. Griffiths, E.J.R. van Beek, J.M. Wild, Investigating 3He diffusion NMR in the lungs using finite difference simulations and *in vivo* PGSE experiments, J. Magn. Reson. 167 (2004) 1.

[24] B. Sapoval, M. Filoche, E.R. Weibel, Smaller is better—but not too small: a physical scale for the design of the mammalian pulmonary acinus, PNAS 99 (2002) 10411.

[25] M. Felici, M. Filoche, B. Sapoval, Diffusional screening in the human pulmonary acinus, J. Appl. Physiol. 94 (2003) 2010.

[26] M. Felici, B. Sapoval, M. Filoche, Renormalized random walk study of oxygen absorption in the human lung, Phys. Rev. Lett. 92 (2004) 068101.

[27] M. Felici, M. Filoche, C. Straus, T. Similowski, B. Sapoval, Diffusional screening in real 3D human acini—a theoretical study, Resp. Physiol. Neurobiol. 145 (2005) 279.

[28] D.S. Grebenkov, M. Filoche, B. Sapoval, M. Felici, Diffusion-reaction in branched structures: theory and application to the lung acinus, Phys. Rev. Lett. 94 (2005) 050602.

[29] American Thoracic Society, Standards for the diagnosis and care of patients with chronic obstructive pulmonary disease, Am. J. Respir. Crit. Care Med. 152 (1995) S77.

[30] C. Butler, Lung surface area in various morphologic forms of human emphysema, Am. Rev. Respir. Dis. 114 (1976) 347.

[31] B.M. Wiebe, H. Laursen, Lung morphometry by unbiased methods in emphysema: bronchial and blood vessel volume, alveolar surface area and capillary length, APMIS 106 (1998) 651.

[32] H. Kitaoka, S. Tamura, R. Takaki, A three-dimensional model of the human pulmonary acinus, J. Appl. Physiol. 88 (2000) 2260.

[33] M. Freidlin, Functional Integration and Partial Differential Equations, Annals of Mathematics Studies Princeton University Press, Princeton, New Jersey, 1985.

[34] D.S. Grebenkov, NMR survey of the reflected Brownian motion, Rev. Mod. Phys. (submitted for publication).

[35] C.P. Bidinosti, J. Choukeife, P.-J. Nacher, G. Tastevin, *In vivo* NMR of hyperpolarized 3He in the human lung at very low magnetic fields, J. Magn. Reson. 162 (2003) 122.

[36] W. Feller, 2nd ed.An Introduction to Probability Theory and Its Applications, Vol. I and II, John Wiley & Sons, New York, 1971.

[37] R.S. Fraser, N.C. Colman, N.L. Muller, P.D. Pare, Synopsis of Diseases of the Chest, 3rd ed., Sauders, Philadelphia, 2005.

[38] J.B. West, Physiologie Respiratoire, HRW, Montréal, 1975.

[39] J. Comroe, Physiology of Respiration Chicago, Year book medical publishers, 1965.

[40] D.S. Grebenkov, G. Guillot, Numerical MRI of the translational diffusion in branching three-dimensional labyrinths of a model pulmonary acinus, MAGMA 18 (2005) S128 (# 219).

[41] P.T. Callaghan, A Simple matrix formalism for spin echo analysis of restricted diffusion under generalized gradient waveforms, J. Magn. Reson. 129 (1997) 74.

[42] A.V. Barzykin, Theory of spin echo in restricted geometries under a step-wise gradient pulse sequence, J. Magn. Reson. 139 (1999) 342.

[43] A.L. Sukstanskii, D.A. Yablonskiy, Effects of restricted diffusion on MR signal formation, J. Magn. Reson. 157 (2002) 92.

[44] B. Robertson, Spin-echo decay of spins diffusion in a bounded region, Phys. Rev. 151 (1966) 273.

[45] C.H. Neuman, Spin echo of spins diffusion in a bounded medium, J. Chem. Phys. 60 (1974) 4508.

[46] D.S. Grebenkov, G. Guillot, Localization regime of restricted diffusion in a model pulmonary acinus, in: Proceedings of the Fourteenth ISMRM Meeting, #1624, Seattle, USA, 2006.

[47] S.D. Stoller, W. Happer, F.J. Dyson, Transverse spin relaxation in inhomogeneous magnetic fields, Phys. Rev. A 44 (1991) 7459.

[48] T.M. de Swiet, P.N. Sen, Decay of nuclear magnetization by bounded diffusion in a constant field gradient, J. Chem. Phys. 100 (1994) 5597.

[49] M.D. Hürlimann, K.G. Helmer, T.M. de Swiet, P.N. Sen, C.H. Sotak, Spin echoes in a constant gradient and in the presence of simple restriction, J. Magn. Reson. A 113 (1995) 260.

[50] J.C. Woods, D.A. Yablonskiy, K. Chino, T.S.K. Tanoli, J.D. Cooper, M.S. Conradi, Magnetization tagging decay to measure long-range 3He diffusion in healthy and emphysematous canine lungs, Magn. Reson. Med. 51 (2004) 1002.

[51] C. Wang, G.W. Miller, T.A. Altes, E.E. de Lange, J.P. Mugler III., Time Dependence of 3He Diffusion in the Human Lung: Measurement in the Long-time Regime Using Stimulated Echoes, in: Proceedings of the Fourteenth ISMRM, # 1312, Seattle, USA, 2006.

[52] R.R. Mercer, Alveolar septal structure in different species, J. Appl. Physiol. 77 (1994) 1060.

[53] D. Habib, D.S. Grebenkov, X. Maître, L. De Rochefort, E. Durand, G. Guillot, Experimental study of gas diffusion in a pulmonary acinus model, in: Proceedings of the Fourteenth ISMRM Meeting, #1323, Seattle, USA, 2006.